Computational Investigation of Hydro-Mechanical Effects on Transmissivity Evolution During the Initial Injection Phase at the Desert Peak EGS Project, NV

Benato S.[1], Reeves M.[1], Parashar R.[1], Davatzes N.[2], Hickman S.[3], Elsworth D.[4], Taron J.[3], Spielman P.[5]

1) Division of Hydrologic Sciences, Desert Research Institute, Reno, NV, 89512 USA; 2) Temple University, Philadelphia, PA, 19122 USA; 3) U.S. Geological Survey, Menlo Park, CA, 94025 USA; 4) Pennsylvania State University, University Park, PA, 16802 USA; 5) Ormat Nevada Inc., Reno, NV, 89511 USA

Contact Information:
STEFANO BENATO
PhD Graduate Research Assistant. Geo-Engineering Program
Division of Hydrologic Sciences, DESERT RESEARCH INSTITUTE
2215 Raggio Parkway, Reno, NV 89512 - USA Office: +1 775-673-7647
stefano.benato@dri.edu

ABSTRACT

The low-flow-rate injection phase of an *Engineered Geothermal System* (EGS) experiment in Desert Peak well 27-15 produced increased injectivity at wellhead pressures less than the minimum principal stress. Discrete fracture network simulations, based on fracture/fault attributes measured downhole and at the surface, were used to derive equivalent permeability tensors and preferred fluid migration directions. FLAC^{3D}, a hydro-mechanical simulator, was used to investigate changes in stress and displacement according to perturbations in pore pressure. Although almost all of the seismicity observed during EGS stimulation occurred during the high-flow-rate tensile stimulation phase, we use this seismicity to illuminate the geometry of large-scale geologic structures that could also have served as preferential flow paths during shear stimulation.

INTRODUCTION

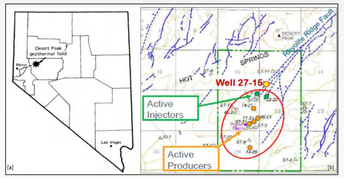

***Fig. 1**: Desert Peak 1) location (from Benoit et al., 1982; b) geothermal field (from Drakos, 2010)*

The Desert Peak geothermal field is a successfully operating geothermal field with an approximate 23 MWe output located in the northern portion of the Hot Springs Mountains of northwestern Churchill County, Nevada, about 100 km northeast of Reno. Well 27-15 was selected to carry out a U.S. Department of Energy supported EGS project with the intent of improving the hydraulic connection with the rest of the reservoir and enhancing overall injectivity. Well 27-15 was originally drilled to a total depth of about 1771m. In 2010 it was back-filled to a total depth of about 1067m, with the completed open-hole section extending from 914m to 1067m to provide a short interval to stimulate through hydraulic and chemical methods [1].

Hydraulic stimulation carried out in Desert Peak well 27-15 from September 2010 through April 2011 led to a nearly 60-fold increase in injectivity [1]. An initial period of shear stimulation, which increased injectivity by more than one order of magnitude, from ~0.011 to ~0.15 gpm/psi, was carried at low fluid pressures up to 4.5 MPa well head pressure (WHP).

This phase was followed by a large-volume controlled hydraulic fracturing operation, which was carried out at high injection rates and WHP in excess of the least principal stress. This hydraulic fracturing stage resulted in an additional 4-fold increase in injectivity [1].

Temperature-Pressure-Spinner logs show that the injected fluid exited and stimulated well 27-15 at two primary locations: 1) the bottom of the open-hole section during the low-flow-rate injection phase and 2) the hydraulic fracture just below the casing shoe during the high-flow-rate injection phase.

During the EGS experiment, a total of 42 micro-earthquakes (MEQs) with magnitudes ranging from +0.10 to +0.74 were recorded between EGS well 27-15 and injection/production wells to the south-southwest, ***(Fig. 2, 3)*** [1]. All but one of these MEQs occurred during the controlled hydraulic fracturing stimulation, with only one event occurring during shear stimulation.

During all stimulation stages, the greatest injectivity gains are associated with the initiation or occurrence of these MEQs under either constant or decreasing wellhead pressure ***(Fig. 2)***. This suggests that the MEQs source mechanism is a key physical process controlling the evolution of transmissivity.

Variations in injection rate occurred in wells 21-2 and 22-22 at various times during EGS stimulation. In some cases, this makes it difficult to establish a unique correlation between EGS operations and the observed seismicity.

Poor focal sphere coverage and limited constraints on the seismic velocity model make it difficult to: (1) derive the exact source mechanism for these MEQs, (2) detect events smaller than magnitude M_w < +0.1 or (3) define the location of individual events with precision. Nevertheless, tensile failure produces relatively high frequency signals at the crack tip – typically of M<<0, which can usually only be detected with the use of specialized downhole instruments [16]. Thus, it is likely that the primary process generating MEQ events at Desert Peak is hydraulically-induced shear failure (Mode II-III) along pre-existing natural fractures and faults that are well-oriented for shear failure in the regional stress field (see [2] and [6]).

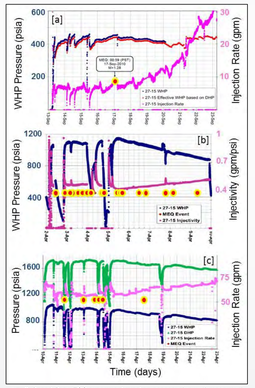

***Fig. 2**: Desert Peak EGS experiment injection phases: a) low, b) medium; c) high injection flow-rates (modified from Chabora et al., 2012)*

The Sept 2010 low-flow-rate stimulation phase is a good candidate for our initial model verification and calibration because: a) injection during this phase occurred at pressures below S_{hmin}, thus only shearing processes were involved, b) the injection rate climbs immediately after a single, yet significant, MEQ event and c) injection into nearby wells 22-1 and 22-22 was relatively steady at the time this earthquake occurred ***(Fig. 2)***.

The first goal of this study is to identify any structure that may provide a high permeability conduit enabling connection to the rest of the field, and appearing to be spatially associated with MEQs during the various stimulation phases (all 42 MEQs).

The second goal of the study is to numerically simulate fluid pressure changes at the location of this MEQ, in response to low-flow-rate injection into 27-15, to establish whether they are sufficient to cause frictional failure.

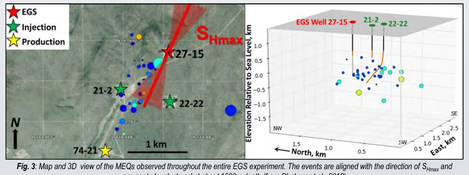

***Fig. 3**: Map and 3D view of the MEQs observed throughout the entire EGS experiment. The events are aligned with the direction of S_{Hmax} and appear to be clustered at about 1500m depth (from Chabora et al., 2012)*

RESERVOIR CONCEPTUAL MODEL

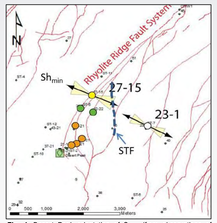

***Fig. 4**: Desert Peak orientation of S_{hmin} (from observations of tensile fractures [2] (Fig. modified from Sweyer et al, 2012). Trace of the Shearing Target Fault (STF) inferred to intersect wells 22-22 and 27-15 at depth shown with a blue dashed line (see below).*

The Desert Peak geothermal field dominant fault pattern trends about N25°E and appears to be related to Basin-and-Range tectonic stresses. The most significant fault in the area is the NNE-trending, WNW-dipping Rhyolite Ridge fault zone, which consists of several strands and steps to the left [4] ***(Fig. 4)***. Orientations of the horizontal principal stresses in well 27-15 were determined through analysis of drilling-induced tensile fractures visible in both high-temperature acoustic televiewer (ABI85) and formation micro-scanner (FMS) logs (S_{hmin} = 114 ± 17° [2].

A 3D analysis of the ES wellsite based on the geologic interpretation proposed by *Faulds et al., 2010* [4] ***(Fig. 6)***, suggests that EGS well 27-15 and injector well 22-22 encounter the same horizon at about 1400m depth, a projection of one of the main Rhyolite Ridge Fault Zone structures mapped at the surface ***(Fig. 4, 6)***. This horizon is near a dense cluster of MEQs associated with injection into well 27-15 and increases in injection rate that were occurring at about the same time into well 22-22.

This seismicity occurs at a depth of 1400 to 1600m, which is significantly below the interval of fluid egress from well 27-15 at a depth of ~914m [1] ***(Fig. 6)***. At 1400m depth, significant fluid loss associated with large-aperture fractures is observed in the deeper section of well 27-15 [2]. Also, in well 22-22, an active injection well located ~400m south of 27-15, major feed zones are found at depths of 790m and 1340m.

Thus, a major NNE-striking and WNW-dipping segment of the Rhyolite Ridge Fault Zone might extend between wells 22-22 and 27-15 and establish a cross-formational hydraulic connection between these two wells. This structure appears to represent a preferential flow path for fluids circulating in its vicinity, in addition to being well oriented for shear failure in the current stress field [6] [18].

The single MEQ observed during the Sept 2010 phase is located deeper than the main cluster of MEQs observed throughout the entire EGS experiment ***(Fig. 6)***. However, taking into account significant vertical errors on the order of hundreds of meters for this specific event, the most likely structure which generated the Sept 2010 MEQ remains the STF.

The temporal association of high-pressure injection into 27-15 during the controlled hydrofrac phase and this cluster of seismicity suggest that EGS stimulation caused some of this seismicity. However, concurrent increases in the injection rate into well 22-22 immediately before high-pressure injection makes it difficult to establish a unique causal link between most of this seismicity and EGS stimulation.

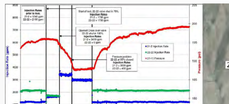

***Fig. 5**: Transient testing conducted by altering injection rates in wells 22-22 and 21-2 while observing pressure response in well 27-15. The test shows that well 27-15 is weakly but mainly connected with well 22-22 (Fig. modified from Drakos et al., 2010).*

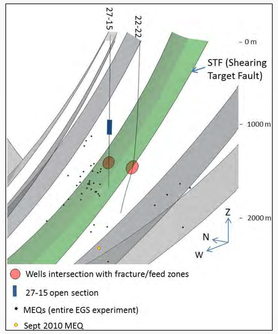

***Fig. 6**: Conceptual model of the major fault strands of the EGS wellsite (inferred from the geologic interpretation introduced by Faulds et al., 2010). The three-dimensional geometry allows for the visualization at depth of MEQs (occurred within the span of the entire EGS experiment) with respect to the structural setting. Both wells 27-15 and 22-22 encounter a highly-fractured and permeable horizon (Shearing Target Fault "STF") at about 1400m depth. Most of the MEQs recorded throughout the course of the EGS experiment are clustered at about 1400m-1600m depth, which coincides with the approximate projection at depth of the STF.*

TECHNICAL APPROACH

Discrete Fracture Network Modeling

The data set measured by *Davatzes and Hickman, 2009* [2] from FMS and ABI85 image logs in well 27-15 is used to generate a representative statistical fracture network ***(Fig. 7)*** to simulate the corresponding fluid flow in the rock volume containing the well. TPS anomalies show evidence of 28 flowing fractures along the entire sampled length (778m), 8 of which are along the simulated open-hole section of the well (152m) [2]. Along the same open-hole section, a permeability-thickness of 60 mD-ft was determined [17], yielding an average permeability of 1.2e-16 m^2, a hydraulic conductivity of 4.7e-09 m/s (using reservoir fluid properties for a measured temperature of 120°C: fluid density ρ=948.7 kg/m3, fluid viscosity μ=2.35e-04 Pa-s) and a corresponding average transmissivity of 7.1e-07 m^2/s. Considering 8 flowing fractures along the current open-hole section of the well, the equivalent average transmissivity *T* per flowing fracture becomes 8.9e-08 m^2/s. By applying the cubic law, b = (12μ*T*/ρg)$^{1/3}$, the mean hydraulic aperture *b* is therefore 30μm.

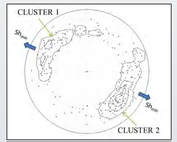

	CLUSTER 1	CLUSTER 2
Quantity	71	114
Cluster Probability	27.2 %	43.7 %
Mean Strike	28.8°	205.4°
Mean dip	58.0°	58.4°
Aperture	50 ft	13.0

***Fig. 7** statistical analysis and parameters used for the generation of the fracture network (2).*

Fracture length is assumed to be distributed according to a power-law: $P(L > 1) = Cl^{-a}$, where a power-law exponent of *a*=2, corresponding to the approximate average of power-law exponents measured in the field [15] was selected to represent fracture length in the DFN model. The resulting fracture lengths are then scaled to the fracture heights using [10]: $H = \frac{L}{2.2}$, where *H* and *L* are the fault height and length, respectively.

A three-dimensional DFN is reproduced [14] where fractures are seeded as: 1) fracture location via a random point process, 2) orientation via a Fisher distribution consistent with prior probabilities for each set, 3) fracture lengths by input of the *a*=2 value through a Pareto distribution truncated to censor extreme values greater than 200 m; and 4) a lognormal distribution of fracture transmissivity. The latter is derived as follows: only 8 of 261 fractures (~3%) were found to be significantly conductive, which we define as having a hydraulic aperture greater than 100μm from the well-test analysis presented above. Using a mean fracture aperture of 30μm derived from the well hydraulic test, fracture variance is changed so that approximately 3% of the fractures have an aperture greater than 100μm. The upper and lower bounds of the distribution are then censored to avoid computational problems with apertures being too small (< 2μm) and to retain realness by not allowing apertures to be unreasonably large (>500μm).

Flow is then solved iteratively via a biconjugate gradient method under specific boundary conditions at all internal nodes according to Darcy's law [3][8][12][13][11].

FLAC^{3D} Fluid-Mechanical Response Model

The conceptual model is tested against the September 13 to 23, 2010, low-flow-rate injection phase (FIG 1) by numerical simulation with the mechanical-flow code FLAC^{3D}. This simulation consists of two successive stages: (1) hydraulic-only computation of pressure gradients generated between the STF and the stimulation interval during fluid injection, and (2) a hydro-mechanically coupled calculation to estimate the mechanical deformation in response to increased hydraulic pressure within the STF, where changes in pore pressure generate deformation, and volumetric strain causes pore pressures to evolve.

The timing at which this single MEQ occurred during the Sept 2010 phase represents a perfect reference for model calibration as it defines the diffusion time required by the hydraulic pressure to build-up to a value critical for triggering mechanical deformation (i.e. shear failure) in the rockmass. Therefore, we tune the model of pressure diffusion through the fracture network between the open-hole interval in 27-15 and the location of the MEQ to determine the model parameters/conditions necessary to cause an MEQ 4 days after the initiation of injection into 27-15 at WHP fluid pressures of ~3.2MPa.

TABLE 2a	Rock type a, b	Rock type c
Density [g/cm^3]	2.5	2.5
Shear Modulus [MPa]	1.0E+04	1.0E+04
Bulk Modulus [MPa]	1.7E+04	1.7E+04
Friction angle [°]	39.1	21.0
Cohesion [MPa]	20.6	0
Tensile strength [MPa]	1.0E+04	1.0E+04

TABLE 2b	kx [m^2]	ky [m^2]	kz [m^2]	Porosity φ
Rock type a	1.4e-16	1.4e-16	7.2e-18	0.01
Rock type b	1.9e-17	1.9e-17	7.0e-17	0.01
Rock type c (27-15 end)	7.0e-18	1.0e-17	1.9e-14	0.01
Rock type c (22-22 end)	7.0e-16	2.3e-14	9.4e-17	0.01

***Table 2**: Parameters used in FLAC^{3D} model; a) rock mechanics, b) hydraulic.*

In the simplified representation of the wellsite, the model comprises a low permeability background formation (rock type a), a formation in the vicinity of the open hole (rock type b), and a fault zone (STF, rock type c). The grid is discretized into regular zones 100m on a side. The STF - like the rest of the model - is currently assumed to be a fluid-saturated single-porosity media. Later modeling exercises and coupling with TOUGHREACT may adopt a dual-porosity conceptualization.

The permeability assigned to the formation surrounding well 27-15 in the FLAC^{3D} model is guided by DFN equivalent permeability tensors. The highest permeability values are assigned to the STF, within which both the vertical and horizontal tensors vary according to a prescribed gradient between well 27-15 (STF north end) and well 22-22 (STF south end) ***(Table 2b)***.

Xx, zz and yy stress components vary with depth following the relations between S_{hmin}, S_{Hmax} and S_v (vertical overburden): $S_{Hmax} = (S_{hmin} + S_v)/2$ [6]. A Mohr-Coulomb plasticity constitutive model is used in FLAC^{3D} to properly represent the onset of shear (frictional).

The mechanical parameters used in the model are derived from rock mechanical tests conducted on selected core samples representative of the stimulation interval in well 27-15 [9] ***(Table 2a)***. The STF is set with zero cohesion, as in-situ stress measurements in a variety of tectonically-active geologic settings suggest that fracture planes well oriented with respect to the stress field are generally cohesionless [5][19].

With reference to the Sept 2010 low-flow-rate phase, an average volumetric flow rate of 5e-5m^3/s is used for well 27-15, while an average volumetric flow rate of 2.5e-5m^3/s is used for the two feed zones in well 22-22: 60% of the injected fluid is prescribed to the deep feed zone, while the remaining 40% is applied to the shallower feed zone, according to TPS logs.

RESULTS

Discrete Fracture Network Modeling

The DFN provides the following horizontal (k_x=east-west, k_y=north-south) and vertical (k_z) average equivalent permeabilities comprising, for the volume containing well 27-15, the permeability tensor k_x=2.50-17m^2, k_y=1.83e-16m^2, k_z=6.16e-17m^2 respectively. The results emphasize preferential flow through k_y and k_x relative to k_z, in accordance with the trends of the major structural features. The existing natural fracture network supports vertical fluid flow and represents a preferential pathway through which injected fluids can reach greater depths.

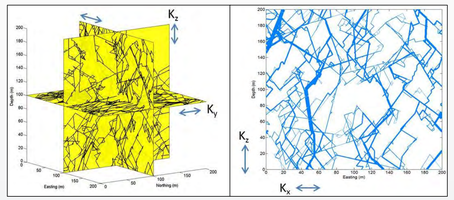

***Fig. 8**: (left) Site representative 3D fault network mapped onto three orthogonal planes of a Cartesian coordinate system along with (right) fault network projected onto x-z plane with line thickness proportional to flow. Only interconnected fault segments of the hydraulic backbone are shown. Note that the frequency of higher permeability fractures is consistent with that encountered in well 27-15 (i.e., approximately 7 fractures over a 200 m vertical length).*

FLAC^{3D} Modeling

Under the Sept 2010 phase conditions, the FLAC^{3D} hydraulic-only simulation shows that fluid diffusion throughout the STF generates a maximum pressure increase of ~1.8 MPa within the STF after about 4 days of injection ***(Fig. 9)***. A Mohr-Coulomb analysis suggests that this maximum pressure increase within the STF is sufficient to generate shear failure in well-oriented, cohesionless fractures ***(Fig. 11)***. The instantaneous downhole pressure response measured in 27-15 during the injection test is simulated through inverse modeling exercises ***(Fig. 12)***. The FLAC^{3D} hydro-mechanical coupled analysis predicts shear failure within the STF after about 4 days of injection into the stimulation zone of well 27-15 ***(Fig. 10)***.

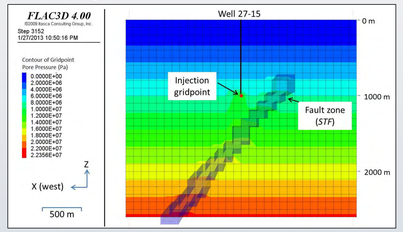

***Fig. 9**: The Sept 2010 low-flow-rate EGS injection phase is simulated in a FLAC^{3D} hydraulic-only analysis by applying constant injection of fluid (5e-5m^3/s) at the injection gridpoint (closest point to the casing shoe of the well) during EGS stimulation. Fluid diffusion through natural fracture networks from the injection point toward greater depths increases the pore pressure within the more permeable STF. Maximum pressure increase (i.e delta P) simulated within the STF is 1.80 MPa.*

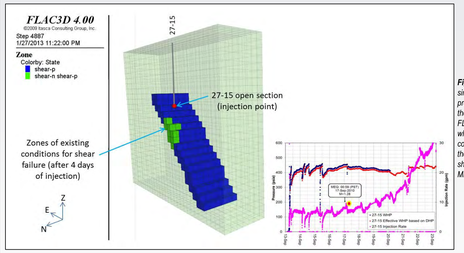

***Fig. 10**: FLAC^{3D} coupled hydro-mechanical simulation of mechanical response as a result of pressure increase generated along the STF during the Sept 2010 low-flow-rate EGS injection phase. FLAC^{3D} displays zones of the model (i.e. STF) where the pore pressure incremental establishes conditions for initiation of plastic flow (i.e. shear-n > the zone is at active failure now, -n). Conditions for shear failure occur after 4 days of injection, when the MEQ was also observed.*

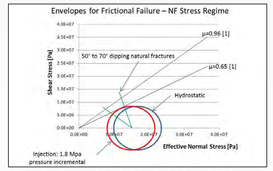

***Fig. 11**: Normal-stress regime Mohr circles showing shear and effective normal stress at 1600m depth (location of MEQs and STF) under: 1) hydrostatic conditions (blue circle) and 2) hydraulic pressure generated along the STF after 4 days of fluid injection in 27-15 (red circle), using pressure increase derived from the FLAC^{3D} hydraulic model (Sept 2010 low-flow-rate phase hydraulically-induced conditions). Frictional failure lines are based on the coefficient of sliding friction derived from [9]. In-situ natural and cohesionless fractures are well-oriented and critically stressed for shear failure.*

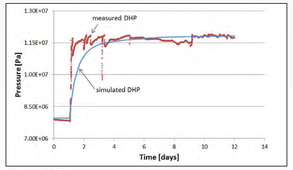

***Fig. 12**: FLAC^{3D} simulated downhole pressure against measured downhole pressure response observed in well 27-15 during the Sept 2010 low-flow-rate EGS injection phase. This is a promising sign that the correct calibration of the FLAC^{3D} model has been achieved.*

DISCUSSION AND CONCLUSION

The modeling results (i.e. migration of injected fluid at depth, pressurization and shearing of the STF) appear to validate the hypothesis that the proposed framework (based on the identification of the STF) is a plausible explanation for the presumed correlation between the observed injection rate increase and the occurrence of microseismicity at depths greater than the open section. Related physical processes have been inferred in several injection-disposal operations, especially along faults that transit between basement rocks and overlying aquifers. Such a process may have been responsible for recent observations of injection-induced seismicity at Guy, Arkansas [7]. Given the non-uniqueness of the problem, the presented conceptual framework is one possible model for the Desert Peak EGS experiment. Future coupling with TOUGHREACT will be carried out to better understand the evolution of permeability associated also with thermal, tensile and chemical processes throughout all phases of the Desert Peak EGS stimulation.

ACKNOWLEDGMENTS

This work is supported by the Great Basin Center for Geothermal Energy under a Geothermal Technology Program (GTP) Faculty Seed Grant, Ormat Technologies, Inc., and Itasca through the Itasca Education Partnership program.

REFERENCES cited in this poster

1) Chabora, E., Zemach, E., Spielman, P., Drakos, P., Hickman, S., Lutz, S., Boyle, K., Falconer, A., Robertson-Tait, A., Davatzes, N.C., Rose, P., Majer, E., Jarpe, S., (2012), Hydraulic stimulation of well 27-15, Desert Peak Geothermal Field, Nevada, USA, *Proceedings, 37th Workshop on Geothermal Reservoir Engineering*, Stanford University, Stanford, California, January 30 - February 1, 2012, SGP-TR-194.
2) Davatzes, N.C. and Hickman, S., (2009), Fractures, stress and fluid flow prior to stimulation of well 27-15, Desert Peak, Nevada, EGS project, *Proceedings, 34th Workshop on Geothermal Reservoir Engineering*, Stanford University, Stanford, California, February 9-11, 2009 SGP-TR-187.
3) de Dreuzy, J.R. & Erhel, J., (2003), Efficient algorithms for the determination of the connected fracture network and the solution to the steady-state flow equation in fracture networks, *Comput. Geosci.*, Vol. 29, No. 1, 107–111.
4) Faulds, J.E., Coolbaugh, M.F., Benoit, D., Opplinger, G., Perkins, M., Moeck, I., Drakos, P., (2010), Structural controls of geothermal activity in the Northern Hot Spring Mountains, Western Nevada: the tale of three geothermal systems (Brady's, Desert Peak, and Desert Queen), *Geothermal Resources Council Transactions*, Vol. 34, 2010.
5) Hickman, S (1991), Stress in the lithosphere and the strength of active faults, *U.S. National Report to the International Union of Geodesy and Geophysics 1987-1990, Reviews of Geophysics*, v. 29, p. 759-775.
6) Hickman, S. and Davatzes, N.C., (2010), In-situ stress and fracture characterization for planning of an EGS stimulation in the Desert Peak Geothermal field, Nevada, *Proceedings, 35th Workshop on Geothermal Reservoir Engineering*, Stanford University, Stanford, California, February 1-3, 2010 SGP-TR-188.
7) Horton, S., (2012), Disposal of hydrofracking waste fluid by injection into subsurface aquifers triggers earthquake swarm in central Arkansas with potential for damaging earthquake, *Seismological Research Letters*, Vol. 83, Number 2, March/April 2012.
8) Klimczak, C., Schultz R.A., Parashar R., Reeves D.M., (2010), Cubic law with correlated aperture to length and implications for network scale fluid flow, *Hydrogeology Journal*, doi:10.1017/s10040-009-0572-6.
9) Lutz, S.J., Hickman, S., Davatzes, N., Zemach, E., Drakos, P., Robertson-Tait, A., (2010), Rock mechanical testing in support of well stimulation activities at the desert Peak geothermal field, Nevada, *Geothermal Resources Council Transactions*, Vol. 34, 2010.
10) Nicol, A., Watterson, J., Walsh, J., Childs, C., (1996), The shapes, major axis orientations and displacement patterns of fault surfaces, *Journal of Structural Geology*, Vol. 18, No. 2/3, pp. 235 to 248, 1996.
11) Parashar, R. and Reeves D.M. (2012), On iterative techniques for solving flow in large two-dimensional discrete fracture networks, *Journal of Computational and Applied Mathematics*, doi:10.1016/j.cam.2012.02.038.
12) Priest, S.D., (1993), *Discontinuity Analysis of Rock Engineering*, Chapman and Hall, London.
13) Reeves, D.M., Parashar, R., Zhang, Y., (2012), Hydrogeologic characterization of fractured rock masses intended for disposal of radioactive waste, *Radioactive Waste*, Dr. Rehab Abdel Rahman (Ed.), ISBN: 978-953-51-0551-0, InTech.
14) Reeves, D.M., Pohll, G., Lyles, B., Faulds, J., Louie, J., Ehni, B., Kratt, C., Cooper, C., Parashar, R., Pullammanappalli, S., Noel D., (2012), Geothermal resource characterization and evaluation at Astor Pass, Nevada, *Geothermal Resources Council Transactions*, 36, 1371-1376.
15) Renshaw, C.E. (1999). Connectivity of joint networks with power law length distributions, Water Resour. Res., 35(9), 2661-2670.
16) Sherburn, S. and Quinn, R., (2012), An Assessment of the Effects of Hydraulic Fracturing on Seismicity in the Taranaki Region, *GNS Science Consultancy Report 2012/50*, February 2012.
17) Stacey, R.W., Robertson-Tait, A., Drakos, P., Zemach, E., (2010), EGS stimulation of well 27-15, Desert Peak geothermal field, Nevada, *Geothermal Resource Council Transactions*, Vol. 34, 2010.
18) Sweyer, M.W., Davatzes, N.C., (2012), Using boundary element modeling of fault slip to predict patterns of stress perturbation and related fractures in geothermal reservoirs and explore parameter uncertainty, *Proceedings, Thirty-Seventh Workshop on Geothermal Reservoir Engineering*, Stanford University, Stanford, California, January 30 – February 1, 2012, SGP-TR-194.
19) Townend, J., and Zoback, M. D. (2000), How faulting keeps the crust strong, Geology, v. 28, p. 399–402.